

PAPER • OPEN ACCESS

Measurement and prediction of granite damage evolution in deep mine seams using acoustic emission

To cite this article: Sunwen Du *et al* 2019 *Meas. Sci. Technol.* **30** 114002

View the [article online](#) for updates and enhancements.

You may also like

- [Elastic Wave Velocity and Attenuation Tomography Using Randomly-Induced Excitations for Damage Detection of RC Slab](#)
K Hashimoto, T Shiotani and C Granier
- [\(Digital Presentation\) Lifetime Prediction of SiC Power Module By Using Time-Series Analysis of Acoustic Emission during Power Cycling Test](#)
Zheng Zhang, Hayate Sato, Yasuko Matsubar et al.
- [AE Monitoring of Hydrogen Embrittlement Crack in Maraging Steel](#)
Ippei Shinozaki, Gen Nakayama and Yohei Sakakibara

Measurement and prediction of granite damage evolution in deep mine seams using acoustic emission

Sunwen Du¹, Guorui Feng^{1,5}, Zhixiong Li^{2,3,5} , Thompson Sarkodie-Gyan⁴, Jianmin Wang¹, Zhenjun Ma³ and Weihua Li³ 

¹ College of Mining Engineering, Taiyuan University of Technology, Taiyuan 030024, People's Republic of China

² School of Engineering, Ocean University of China, Tsingdao 266100, People's Republic of China

³ School of Mechanical, Materials, Mechatronics and Biomedical Engineering, University of Wollongong, Wollongong, NSW 2522, Australia

⁴ College of Engineering, University of Texas, 500 W University Ave, El Paso, TX 79968, United States of America

E-mail: fguorui@163.com (G Feng) and zhixiong_li@uow.edu.au (Z Li)

Received 19 February 2019, revised 4 June 2019

Accepted for publication 16 July 2019

Published 3 September 2019



Abstract

With unceasing increase of mining depth and development intensity, mining disasters such as rock burst have been increasing frequently, which often result in catastrophic accidents. Therefore, it is imperative to accurately forecast underground disasters. Previous research has suggested that the combination of drill-hole pressure relief and acoustic emission (AE) monitoring serves as an effective measure method towards the forecasting and prevention of disastrous accidents. However, the AE evolution mechanism of underground rock damages remains a challenge; more specifically, the relationships among the drilling hole positions, depths and diameters, and the stress–strain and AE characteristics of the rocks are discussed little in the literature. In order to bridge this research gap, the particle flow code (PFC2D) is employed to systemically investigate the hidden patterns among the mechanical properties, AE and damage evolution of the rock mass with different positions, depths and diameters of the drilling holes. Analysis results demonstrate that the drilling position influences the rock stress–strain and AE characteristics in the plastic deformation stage and the residual stage while the hole depth affects the drilling process. More specifically, the initial AE strength, AE impact at the peak moment, AE fluctuations and induction time are significantly influenced by the drilling position and depth. Furthermore, the drilling position and depth change the evolution law in the damage acceleration and stable development stages, while the hole diameter has little effect on the AE signal during the rock drilling process.

Keywords: rock burst, acoustic emission, NDT

(Some figures may appear in colour only in the online journal)



Original content from this work may be used under the terms of the [Creative Commons Attribution 3.0 licence](https://creativecommons.org/licenses/by/3.0/). Any further distribution of this work must maintain attribution to the author(s) and the title of the work, journal citation and DOI.

⁵ Author to whom any correspondence should be addressed.

1. Introduction

On account of the intensity associated with the continuous development of the improvement of mineral resources, rock burst and other mining disasters and accidents have increased. Hence, there is a precipitous, urgent requirement for forecasting and identifying these incidents [1, 2].

There is extensive research towards the urgent need for the prevention and control of mining disaster. Numerous publications have contributed to solve the problem of pressure impact. Several subject-matter areas are considered in the study of the mechanism of percussive ground pressure, which may include theories involving strength, stiffness, energy, bursting liability, instability, fractal, fracture, damage, mutation, bifurcation, dissipative structure, and chaos [3–7]. In the study of percussive ground pressure control, there are basically three methods [8–10]: (1) mining optimization (or change mining sequence), which mainly includes optimizing the shape of the roadway and stope, the setting up of permanent pillar, filling, and changing mining order; (2) artificial support, which mainly includes bolt, anchor rope sprayed concrete, steel arch and concrete lining, flexible material support, and small sections into the lane; (3) pretreatment of ground pressure, which includes water injection softening, blasting weakening, cutting and unloading pressure, drilling holes and so on.

Drilling-hole-based pressure relief is among the effective approaches to control the impact of ground pressure, and hence, it has gradually attracted much attention. Liu *et al* [11] investigated the mechanisms of preventing and controlling the impact pressure of large-diameter drilling holes using rock mechanics experiments. Wang *et al* [12] proposed a FLAC3D system to analyze the dynamic effects of the parameters (length, diameter and row spacing) on the stability of the surrounding rock in the deep roadway. Li *et al* [13] studied the effects of the drilling hole unloading pressure in the stress concentration area in a roadway based on ADINA finite element analysis. Wen *et al* [14] studied the influence of the drilling hole diameter and hole spacing on the effect of the drilling hole unloading pressure by using the FLAC3D system. Jia *et al* [15] studied the influence of the diameter, spacing and depth of the drilling hole on the strength of a rock sample and analyzed the sample failure mode using different parameters through laboratory tests. In addition, particle flow PFC software was employed to investigate the crack propagation morphology and crack number of rock samples using different drilling parameters. Furthermore, recent research results demonstrated that the AE signal can reflect the stress–strain characteristics of the rocks during the pressure relief process [16]. Because rocks will radiate acoustic waves in the process of damage, by analyzing the AE signal it is possible to accurately predict pressure relief performance and to effectively control the pressure impact. Without the use of a traditional strain gauge, the sensor installation problem can be solved by an AE data acquisition system. The stability of a rock mass can be monitored by AE evolution law for the purpose of preventing impact pressure [16, 17]. As a result, the AE technique provides promising potential in the application of mining pressure prediction and control. However, very

limited research in the literature has addressed the influence mechanisms of the drilling parameters on AE characteristics as well as the stress–strain characteristics of rocks. In a previous work Jia *et al* [15] found that the diameter, spacing and depth of the drilling hole may significantly change the rock stress–strain characteristics, but they did not use AE sensors in their investigation. It is therefore worth analyzing the effects of the drilling hole parameters on the AE signal and the rock mechanic characteristics.

In order to address the aforementioned challenge, PFC2D is employed to systemically investigate the hidden patterns among the mechanical properties, acoustic emission (AE) and damage evolution in the rock pressure relief process with different positions, depths and diameters of the drilling hole. The innovation of this work lies in understanding the effects of different drilling parameters on the rock pressure relief (such as mechanical and damage characteristics) based on AE analysis. The findings of this research add new insight to understanding the evolution law of rock damages using AE analysis. The research results can provide a theoretical basis for further investigation of rock instability mechanism and may have important practical significance for safe and green mining.

The contributions of this work are described as follows.

- (1) A particle flow rock model, validated by laboratory experiment data, is established using PFC2D to perform AE monitoring on rock damages.
- (2) A hidden pattern among the mechanical properties, AE and damage evolution characteristics is discovered for the granite under different drilling hole positions, depths and diameters.

2. Rock model

2.1. Introduction of particle flow

The particle flow theory was created on the basis of the discrete element method [18], which is suitable for analyzing the fracture mechanisms and large deformation processes of material damage. PFC is a kind of particle flow analysis software, which is able to model discrete particles and the connections among particles. So PFC can simulate the contact fracture mechanics of the particles such as particle bond failure. Compared with other software such as ANSYS (based on finite element method), the contact fracture mode established by PFC is more realistic and suitable to calculate the crack growth (damage evolution) of rock materials. Moreover, even subject to the limitations of particle volume and computation complexity, PFC is still competent for calculation of the contact fracture responses of very small models such as a rock model. Previous works [19–21] have proven the PFC calculation results can be used as a reference for field and indoor tests. As a result, it is reasonable to use PFC software to perform the present research.

In simulating particle bond failure, the particle flow program provides two kinds of bonding models: contact bonding and parallel bonding models, respectively [19]. The contact bonding model considers the bonding of points between

particles, which cannot transfer torque but only force when the particles produce relative displacement. So this kind of bonding model is suitable for bulk materials such as soil. The parallel bonding model considers the bonding between particles, which can transfer torque. So it is suitable for solid materials such as rock. As shown in figure 1, the parallel key can be described as a set of elastic springs that are evenly distributed on the rectangular cross-section at the contact surface of two particles and centered on the contact point [20]. Once the bonding key between two particles breaks, a fracture crack will be generated. The energy change due to the fracture crack in these two particles is used to characterize the AE, that is, a fracture crack will generate an AE and the bonding breaking energy determines the acoustic intensity. In addition, if the distance of multiple fracture cracks is very close, only one AE is produced. In the process of micro-crack propagation inside the rock, the fracture energy will be released as sound waves, i.e. AE by PFC. In this work the parallel bond model in PFC2D was selected to build the rock model to analyze the AE response.

The maximum normal and shear stresses of the bonding key ($\bar{\sigma}$ and $\bar{\tau}$), can be expressed as follows:

$$\begin{cases} \bar{\sigma} = \frac{T}{A} + \frac{|M|\bar{R}}{I} \\ \bar{\tau} = \frac{|V|}{A} + \frac{|M_t|\bar{R}}{J} \end{cases} \quad (1)$$

where A and I are the area of the parallel key section and the rotational inertia; T is the tension; M is the bending moment; M_t is the torque; V is the tangential force. The sectional area of the parallel bond model and rotational inertia can be expressed as follows:

$$\begin{cases} \bar{R} = \min(R^{[A]}, R^{[B]}) \\ A = 2\bar{R}t \\ I = \frac{1}{12}t(2\bar{R})^3 \end{cases} \quad (2)$$

where t is the thickness of the parallel bond model.

2.2. Parameters validation of rock model

PFC uses micromechanical parameters to characterize the mechanical properties of particles and bonding keys. Before establishing the numerical model, the micromechanics parameters of the rock model must be assigned according to the experimental results in laboratory tests. By adjusting the microscopic mechanical parameters of the rock model, a suitable set of parameters can be applied to make the numerical calculation results basically consistent with the experimental measurements. By doing so, the numerical rock model can be regarded as reliable for simulating the fracture mechanics of a real rock.

In order to obtain the desired set of parameters, the simulation conditions should be similar to laboratory test conditions. A trial and error method is usually adopted to adjust the parameters by repeating the simulations and comparing the experiment results. In this paper the parameters presented in [21] that discussed three axial compressive tests of underground water seal oil cave in Huangdao region were used

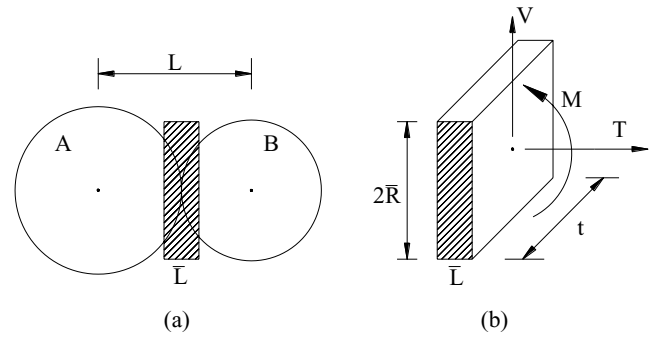


Figure 1. Diagram of 2D parallel bond between particles: (a) parallel-bond idealization, and (b) forces carried in the bond material.

to conduct the numerical simulations. After trial and error processing, a set of microscopic physical mechanics parameters were obtained, as shown in table 1. With these macroscopic mechanical parameters the stress characteristics of the numerical rock model at a confining stress of 6 MPa become consistent with these of the real yellow granite specimens in the same operation conditions. The elastic modulus, Poisson ratio and compressive strength values of the numerical model (granite specimen) are 28.7 GPa (28.4 GPa), 0.2300 (0.2285) and 130.5 MPa (132.8 MPa), respectively. A comparison of the stress–strain curve and failure mode between the numerical model and experimental granite specimen is shown in figures 2 and 3, where the simulation results are consistent with the experiment results.

2.3. Particle-flow-based rock model

When the bonding strength between particles is smaller than the intensity of transmission between the particles, the particle bond will break, i.e. micro-cracks corresponding to the interior of the rock form [22]. In the process of micro-crack propagation inside the rock, the damage energy will be released in AE. Therefore, in the process of rock compression using PFC one can monitor the number of parallel bonding breaks at each time and the bonding break energy to study the AE characteristics of rock damage evolution.

In order to analyze the influence of the drilling hole position, depth and diameter on rock mechanics and AE characteristics, three test groups were designed as illustrated in table 2. The simulation model in each group adopts the same parameters as the above intact rock. Figures 4–6 are models of the three groups, respectively. The effects of particle shape and particle distribution were not considered in this work. By means of the radius expansion method, enough particles were generated in the setting region to satisfy the porosity. After each complete model was generated, some particles were removed according to the test plan. The unbalanced force generated during the model generation was eliminated by circulation. The top wall of the mobile model was loaded and the same strain rate 0.008 mm s^{-1} was applied to the model. In order to prevent the particles from overflowing, the loading wall was properly extended.

Table 1. Physico-mechanical parameters of granite.

Parameter	Value	Parameter	Value
Minimum particle size (mm)	0.3	Normal/tangential stiffness	3.0
Particle size ratio	1.66	Coefficient of friction	0.8
Density (kg m ⁻³)	2800	Parallel bond Normal stiffness (MPa)	88 ± 10
Contact modulus of the particle (GPa)	5.0	Parallel bond tangential stiffness (MPa)	160 ± 10
Deformation of parallel bond modulus (GPa)	43.0		

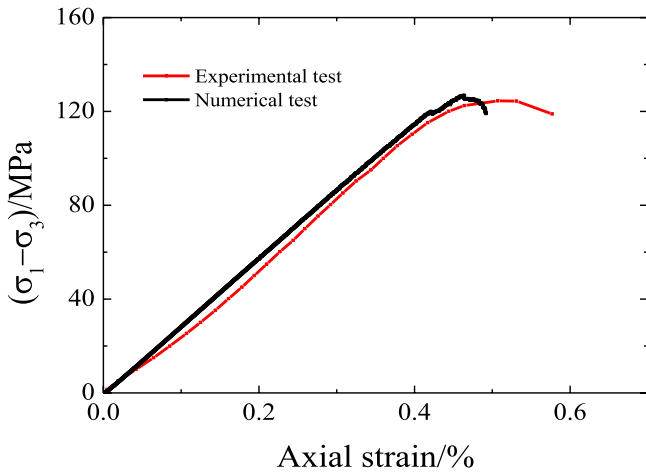


Figure 2. Stress–strain curves of experimental and numerical tests of a granite rock.

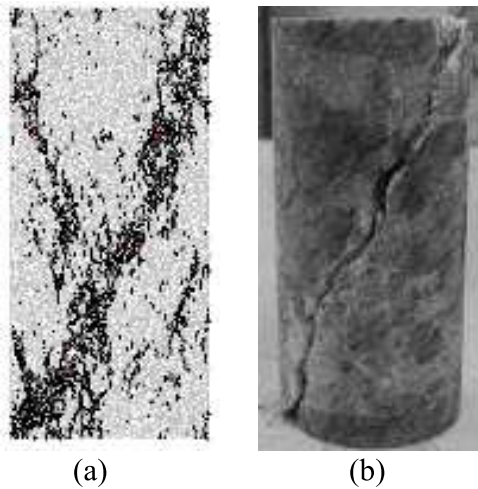


Figure 3. Failure modes of (a) PFC model and (b) real granite in compression at a confining stress of 6 MPa.

3. Numerical analysis result

3.1. Stress–strain characteristics

Figure 7 shows the stress–strain characteristics of the numerical rock model using the parameters in table 1. One can observe that the stress–strain characteristic curve can be divided into three phases. The first stage is the elastic stage, which shows linear relationship between the stress and strain of the rock. The elastic modulus of the rock remains the same in this linear deformation stage. The second one is the plastic deformation stage, which appears at the peak of the rock deformation. In this stage, the stress–strain curve shows

concave characteristics. The third one is the residual damage stage. In this stage, the stress–strain curves show wave form and the stress decreases rapidly as the strain increases.

3.1.1. Influence of the drilling hole position. Figure 8 illustrates the stress–strain characteristics of the numerical rock model with different drilling hole positions (10, 0 and –10 mm). One can observe that the drilling hole position has little influence on the elastic deformation phase of the numerical granite while it exhibits certain influence on the plastic deformation and damage residual phases. With the same drilling hole depth ($D1 = 10$ mm) and diameter ($D2 = 2$ mm), the peak strength and peak strain of the numerical granite decrease with 10 and –10 mm of the drilling hole positions in figure 8, but the elastic modulus remains the same for the three different hole positions. When the drilling hole position is 10 mm, the peak strength and peak deformation of the numerical granite are 96.84 MPa and 0.405%. Compared with the real granite, these values decrease by 16.51% and 14.19%, respectively. When the drilling hole position is 0 mm, the peak strength and peak deformation are 95.90 MPa and 0.389%, decreased by 17.31% and 17.58% respectively to the experimental results. When the drilling hole position is –10 mm, the peak strength and peak deformation are 88.52 MPa and 0.351%, decreased by 23.68% and 25.64%, respectively. From these three-set simulation results one can note that when the drilling hole position is 10 mm, it is closer to the stress loading wall than the other two positions; so the hole is subject to larger stress disturbances, which may increase the deformation speed of the rock, resulting in a higher stress intensity and a large deformation at the peak.

Figure 9 shows the failure mode of the numerical granite model with different drilling hole positions. It can be seen that the angle between the rock primary damage side and horizontal direction increases with the increase of the drilling hole position. When the hole position is 10 mm, the primary damage side is connected to the drilling hole and stretches downward. This explains why its stress–strain curve presents two peaks in figure 8. The first peak is generated when the main surface and the borehole connection are destroyed and the second peak is the destruction of the primary side. When the hole position is 0 and –10 mm, the primary damage side is only connected to the drilling hole but does not stretch downward. Moreover, when $Y = -10$ mm the rock fracture propagates along the primary side and a small crack trace. The small cracks increase the complexity of the stress–strain residual stage.

3.1.2. Influence of the drilling hole depth. Figure 10 shows the stress–strain characteristic curve of numerical granite in

Table 2. Experimental schemes.

Group 1 (position)			Group 2 (depth)			Group 3 (diameter)		
Position (Y)			Depth (D1)			Diameter (D2)		
0 mm	10 mm	2 mm	0 mm	10 mm	2 mm	0 mm	10 mm	2 mm
10 mm	10 mm	2 mm	0 mm	15 mm	2 mm	0 mm	10 mm	3 mm
-10 mm	10 mm	2 mm	0 mm	20 mm	2 mm	0 mm	10 mm	4 mm

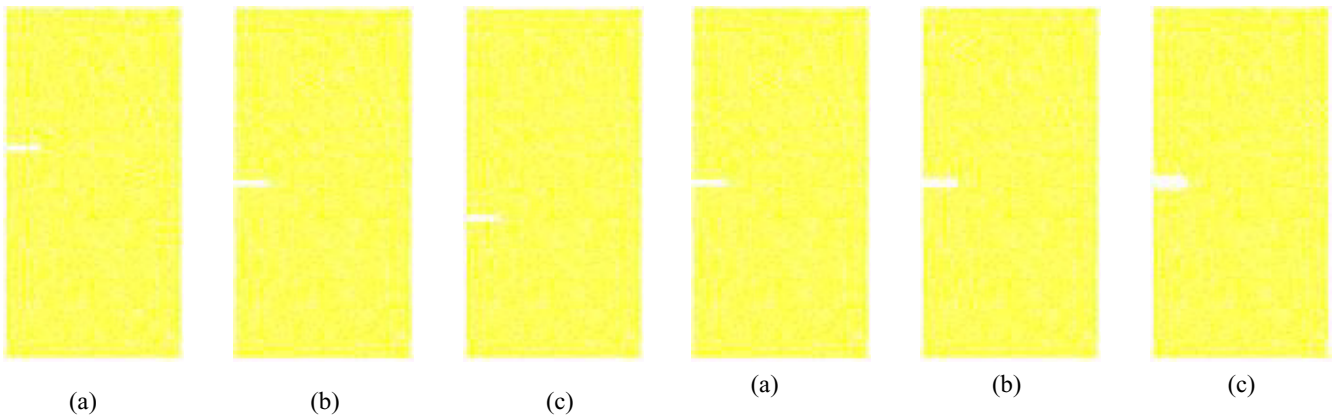


Figure 4. Specimens with different drilling hole positions. (a) $Y = 10$ mm (b) $Y = 0$ mm (c) $Y = -10$ mm.

Figure 6. Specimens with different drilling hole diameters. (a) $D2 = 2$ mm. (b) $D2 = 3$ mm. (c) $D2 = 4$ mm.

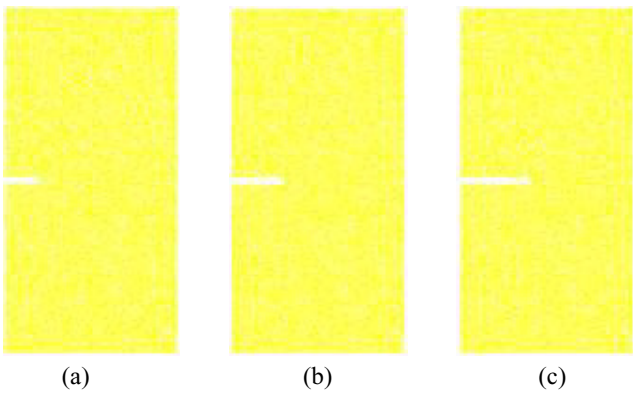


Figure 5. Specimens with different drilling hole depths. (a) $D1 = 10$ mm. (b) $D1 = 15$ mm. (c) $D1 = 20$ mm.

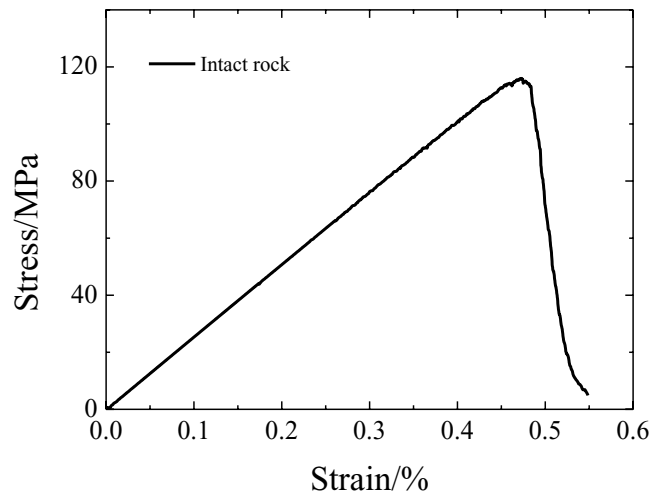


Figure 7. Stress–strain curve of the rock model.

different drilling hole position conditions. It may be observed that the drilling hole depth has certain influence on the elastic stage, plastic deformation stage and the damage residual stage. With the same drilling hole position ($Y = 0$ mm) and drilling hole diameter ($D2 = 2$ mm), the peak strength and elastic modulus of the numerical granite decrease continuously. However, the peak strain shows a tendency to decrease first and then to increase. When the drilling hole depth is 10 mm, the peak strength and elasticity modulus are 95.90 MPa and 24.99 GPa. Compared with the real granite, they decrease by 17.31% and 0.44% respectively. When the depth is 15 mm, the peak strength and elasticity modulus are 84.44 MPa and 23.11 GPa. Compared with the real granite, they decrease by 27.19% and 7.93% respectively. When the depth is 20 mm,

the peak strength and elasticity modulus are 77.26 MPa and 21.32 GPa, decreased by 33.39% and 15.06% respectively. The greater the drilling depth the worse the rock integrity. Larger rock damage results in less compressive strength and elastic modulus of the rock.

Figure 11 shows the failure mode of the numerical granite in different drilling hole depth conditions. It can be seen that the angle between the primary damage side and horizontal direction increases with the increase of drilling depth. The effect of the drilling depth is that the primary damage side is longer with smaller depth while with the increase of the drilling hole depth the fracture width increases.

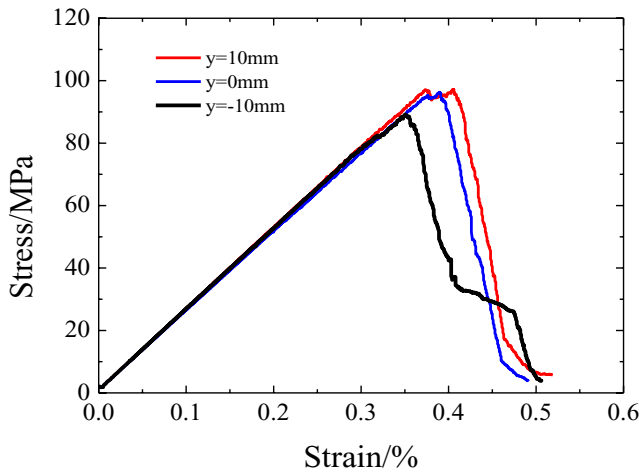


Figure 8. Rock stress–strain curves with different hole positions.

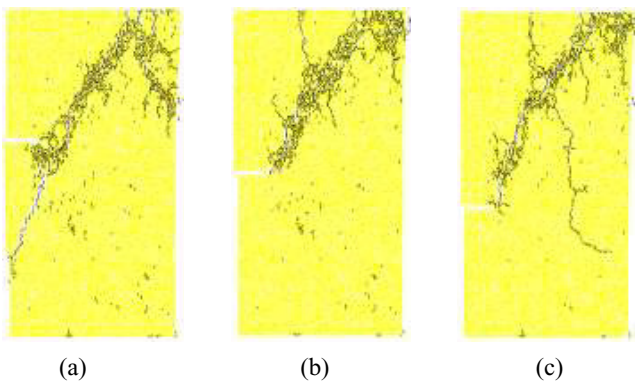


Figure 9. Rock failure mode with different hole positions. (a) $Y = 10$ mm. (b) $Y = 0$ mm. (c) $Y = -10$ mm.

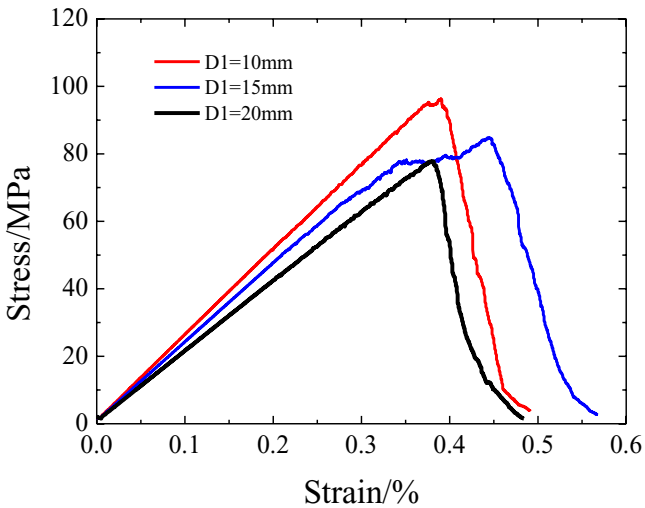


Figure 10. Rock stress–strain curves with different hole depths.

3.1.3. Influence of the drilling hole diameter. Figure 12 shows the stress–strain characteristic curve of the numerical granite in different drilling hole diameter conditions. It can be seen that the drilling hole diameter has limited influence on the fracture process of the numerical granite. With the same drilling hole position ($Y = 0$ mm) and depth ($D1 = 10$ mm), the

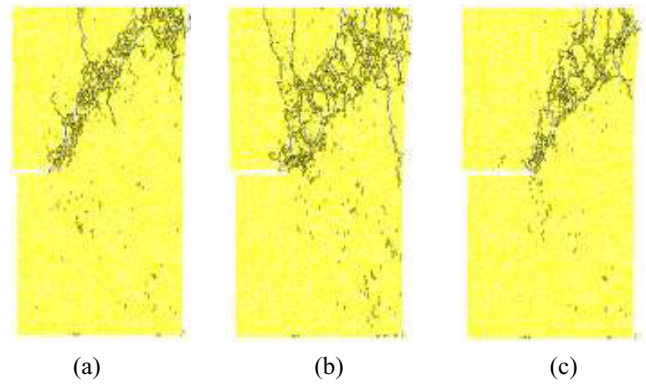


Figure 11. Rock failure mode with different hole depths. (a) $D1 = 10$ mm (b) $D1 = 15$ mm. (c) $D1 = 20$ mm.

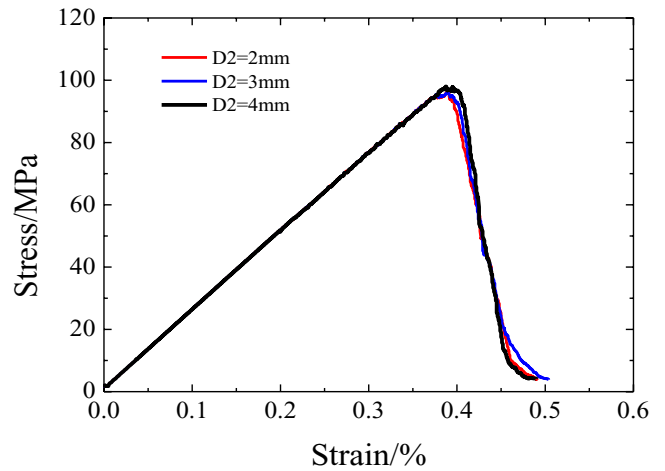


Figure 12. Rock stress–strain curves with different hole diameters.

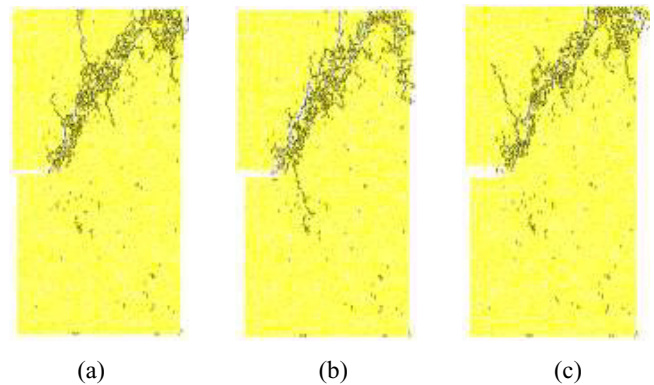


Figure 13. Rock failure mode with different hole diameters. (a) $D2 = 2$ mm. (b) $D2 = 3$ mm. (c) $D2 = 4$ mm.

peak strength and peak strain of the numerical granite slightly increase with increase of the drilling hole diameter and the elastic modulus is basically unchanged. Compared with the drilling hole position and drilling hole depth, the drilling hole diameter is insensitive to the influence of mechanical parameters such as hard rock strength and deformation. In practical engineering, the influence of drill diameter can be ignored. The expected pressure relief effect can be achieved by selecting the proper drilling hole position and depth.

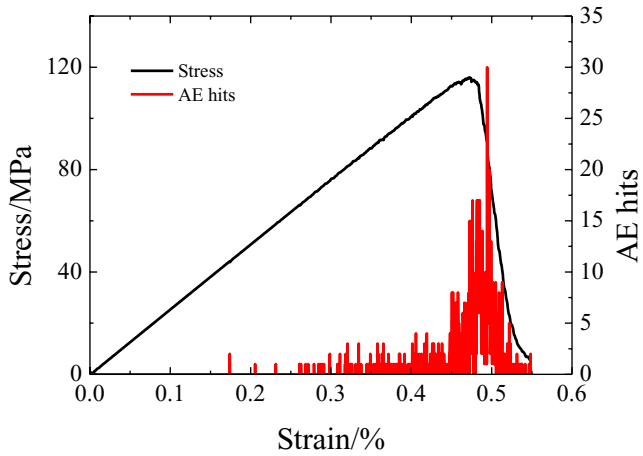


Figure 14. Rock stress–strain-AE hits curve.

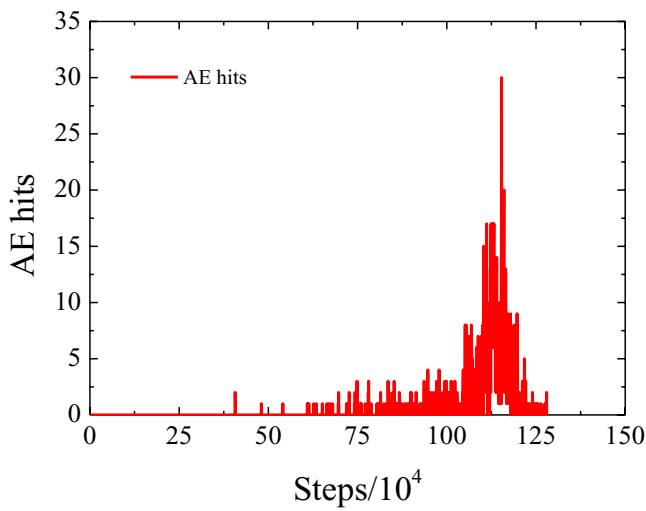


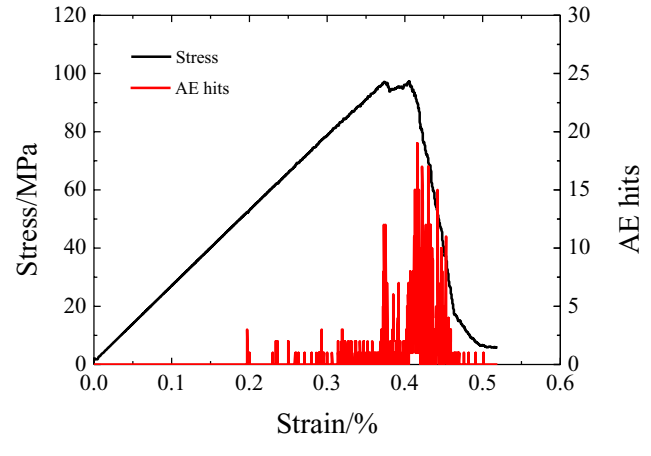
Figure 15. Rock AE hits step curve.

Figure 13 shows the failure mode of the numerical granite with different drilling hole diameters. It can be noticed that the angle between the primary damage side and horizontal direction is almost unchanged.

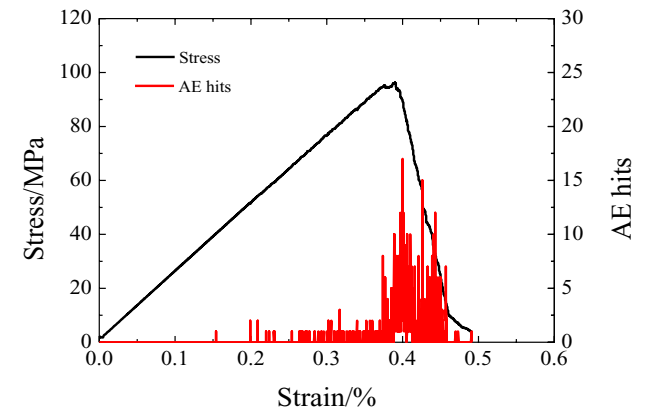
As a result, the rock stress–strain characteristics of different drilling hole positions, depths and diameters are different. The drilling position has the largest influence, followed by the drilling depth, and diameter.

3.2. AE characteristic

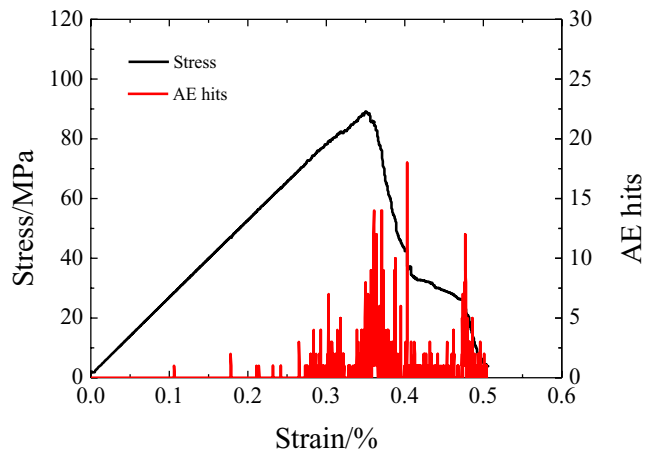
Figure 14 shows the stress–strain-AE hits of the numerical granite, and figure 15 shows the AE hits step curve. In uniaxial compression conditions, the rock AE characteristics are presented as follows. (1) At the elastic stage, the frequency of AE is reduced. This is because as the established model is not fully embossed and closed, there is no AE impact at the initial stage. This is different from the actual rock mechanics AE test. Due to the internal porosity, crack closure and friction, the real rock is often accompanied by a certain AE. (2) At the plastic deformation stage, the rock produces more AE hits. The internal crack of the rock evolves and develops frequently, which is the key stage of rock stability. When the



(a)



(b)



(c)

Figure 16. Rock stress–strain-AE hits curves with different hole positions. (a) $Y = 10\text{mm}$. (b) $Y = 0\text{mm}$. (c) $Y = -10\text{mm}$.

damage reaches a certain level, the rock will be fractured and strong AE signals will be generated. (3) At the residual stage, the internal crack further expands and the AE impact signal rapidly decreases.

3.2.1. Influence of the drilling hole position. Figure 16 illustrates the stress–strain-AE hits curve of the numerical granite in different drilling hole position conditions. One can observe that drilling hole position has a great influence on the AE hits.

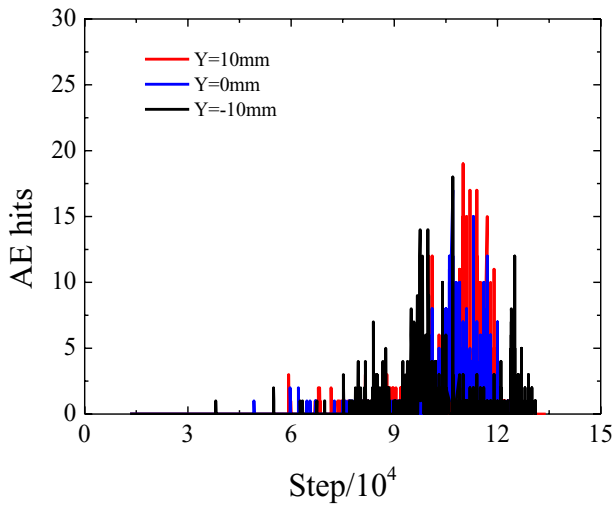


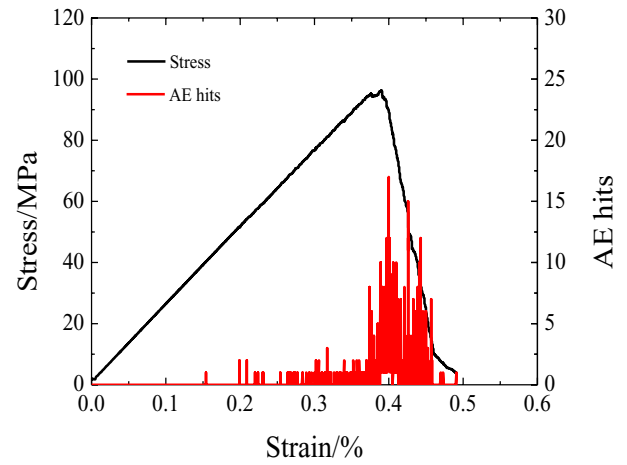
Figure 17. Rock AE hits step curves with different hole positions.

Drilling hole position had an influence on the strain value of the initial AE. When $Y = 10$ mm, the strain value of the initial AE is 0.20%; when $Y = 0$ mm, the strain value is 0.20%; when $Y = -10$ mm, the strain value is 0.11%. Thus, the closer the drilling hole is to the loading wall the more vulnerable the rock is. At the peak time, the AE impact strength decreases with the drilling hole position from top to bottom. When $Y = 10, 0$ and -10 mm, the AE impact strength is 19, 17 and 15 times/step, respectively. At the residual stage the AE hits increases continuously with the drilling hole positions from top to bottom. When $Y = 10, 0$ and -10 mm, the AE impact is about 0.09%, 0.11% and 0.19%, respectively.

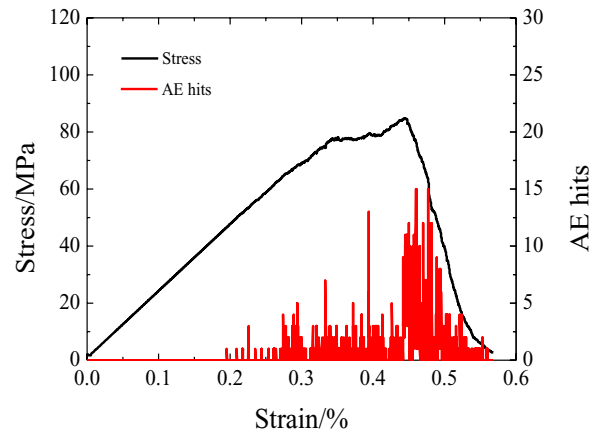
Drilling hole position had an influence on the AE fluctuation rule. When $Y = 10$ mm, the rock changes smoothly at the elastic stage. The AE impact increases after entering the plastic deformation stage. Two peak values are observed in figure 16(a). This rule illustrates the rationality of AE monitoring for the rock damage. After entering the residual stage, the AE impact steadily declines until failure of the rock. When $Y = -10$ mm, the AE fluctuation is close to the real rock. When $Y = 0$ mm, the AE fluctuation is greater than that of $Y = 10$ and -10 mm.

Figure 17 shows the AE hits step curve of the numerical granite in different drilling hole position conditions. It can be seen that the drilling hole position has limited influence on the AE hits but may influence the AE induction time. The induction time decreases with the drilling hole position from top to bottom. When $Y = 10, 0$ and -10 mm, the AE induction time is 59 260, 49 321 and 38 315 steps. Moreover, the drilling position influences the AE maximum impact point, respectively. The impact time has a tendency to increase first and then to decrease with the drilling hole position from top to bottom. When $Y = 10, 0$ and -10 mm, the AE maximum impact point is located at steps 109 992, 113 253 and 106 919, respectively.

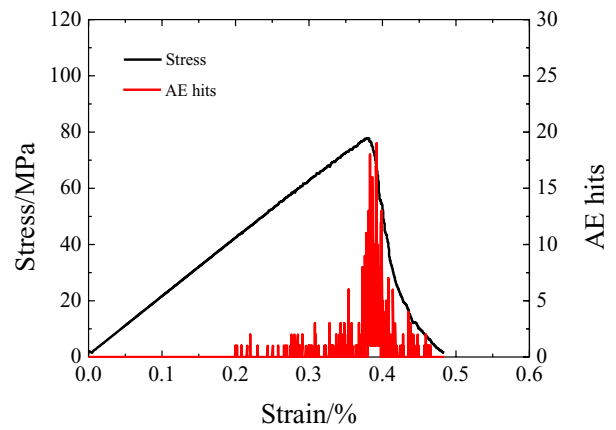
3.2.2. Influence of the drilling hole depth. Figure 18 shows the stress–strain–AE hits curve of the numerical granite in different drilling hole depth conditions. It can be seen that the influence of the drilling hole depth on the AE hits is obvious.



(a)



(b)



(c)

Figure 18. Rock stress–strain–AE hits curves with different hole depths. (a) $D1 = 10$ mm. (b) $D1 = 15$ mm. (c) $D1 = 20$ mm.

The greater the drilling hole depth the greater the rock fracture. At the elastic stage, there is no internal crack generation. At the peak time, the AE intensity increases with the increase of the drilling hole depth. At the residual stage, the AE intensity decreases with the increase of the drilling hole depth.

Figure 19 depicts the AE hits step curve of the numerical granite in different drilling hole depth conditions. One can

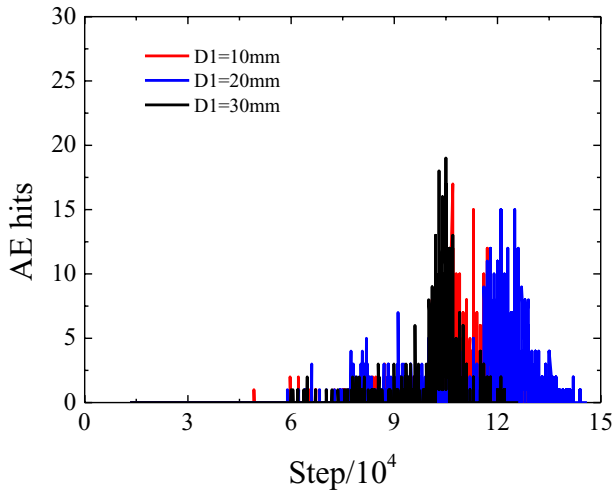


Figure 19. Rock AE hit-steps curves with different hole depths.

observe that the influence of the drilling hole depth on the evolution rule of AE hits step curve is small, but there is a certain effect on the point of AE peak impact. The AE time period is also different with different depths.

3.2.3. Influence of the drilling hole diameter. Figure 20 illustrates the stress–strain–AE hits curve of the numerical granite in different drilling hole diameter conditions. One can observe that drilling hole diameter has little effect on the stress–strain–AE hits curve. Figure 21 shows the AE hits step curve of the numerical granite with different drilling hole diameters. It can be seen that the evolution rule of AE hits step curve is almost the same with different drilling diameters.

Based on these analysis results, the AE characteristics will be influenced by different drilling hole positions, depths and diameters. The influence importance order is drilling position, depth and diameter.

4. Damage evolution characteristics

4.1. Failure model based on AE impact parameters

A large number of studies have shown that the AE impact parameter can reflect the change of material performance. It is proportional to the strain energy released by the dislocation motion, fracture and crack propagation in the material [23, 24]. Therefore, this paper describes the evolution characteristics of rock damage using AE analysis.

Kachanov [25] defined the damage variable as

$$D = \frac{A_d}{A} \tag{3}$$

where A_d is the material damage section area at a given moment; A is the sectional area at the initially moment when the material is free of damage.

Assuming that the cumulative AE frequency is K_0 , when the carrying capacity is completely lost the AE accumulative count K_w is

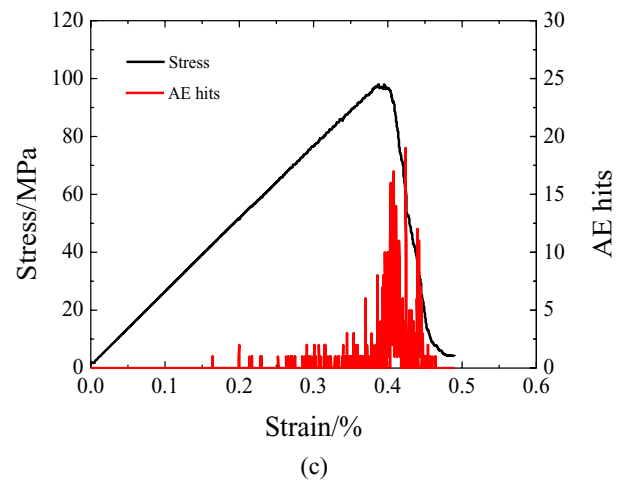
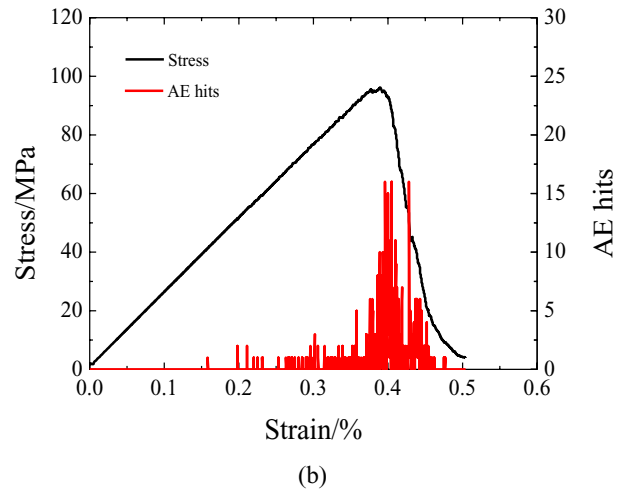
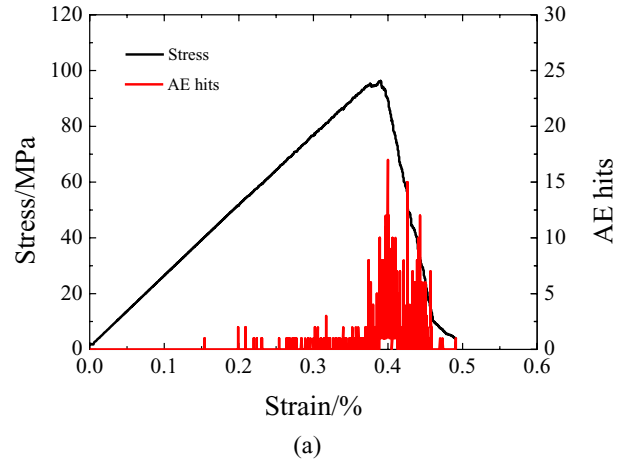


Figure 20. Rock stress–strain–AE hits curves with different hole diameters. (a) $D_2 = 2$ mm. (b) $D_2 = 3$ mm. (c) $D_2 = 4$ mm.

$$K_w = \frac{K_0}{A}. \tag{4}$$

When the rock fracture surface damage reached A_d , the corresponding AE accumulative count K_d is

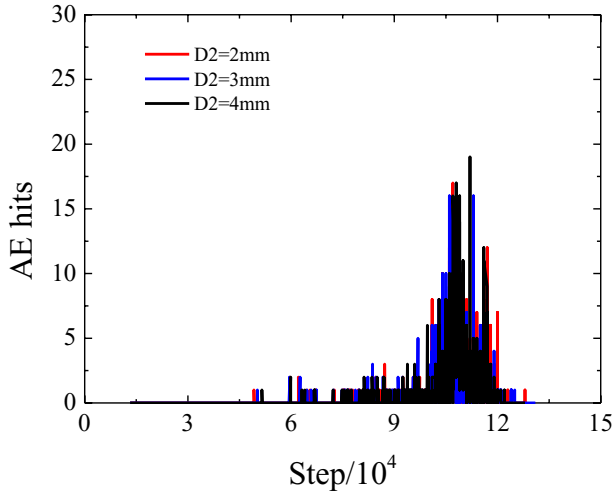


Figure 21. Rock AE hits step curves with different hole diameters.

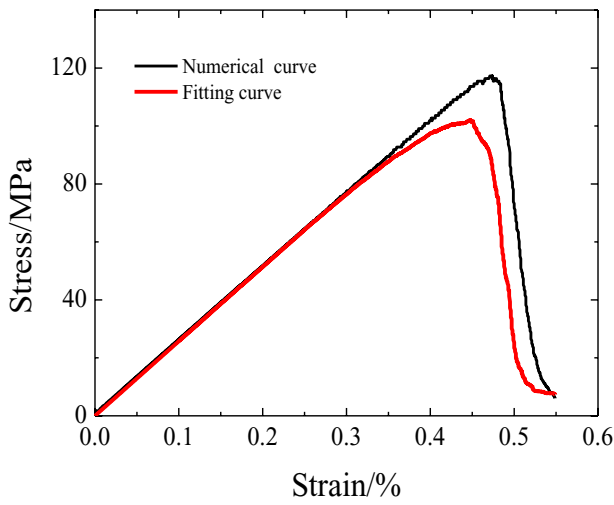


Figure 22. Stress-strain curves based on equation (9).

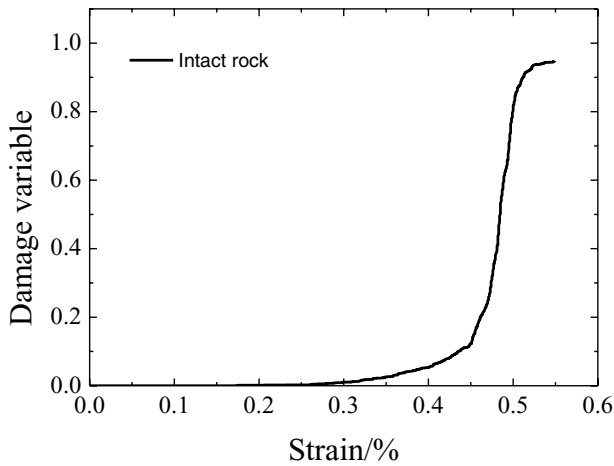


Figure 23. Damage variable-strain curve.

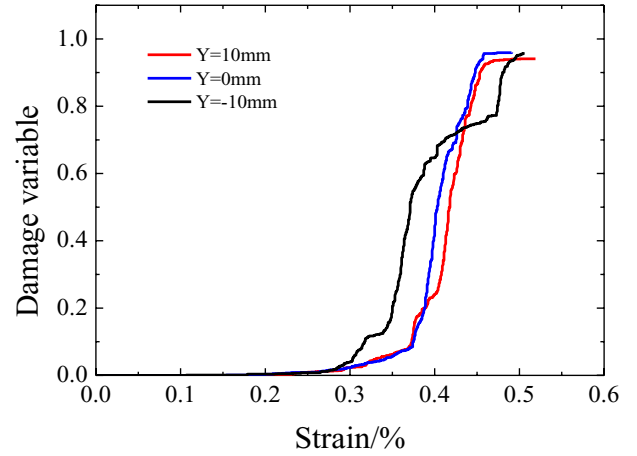


Figure 24. Damage variable-strain curves of specimens with different borehole positions.

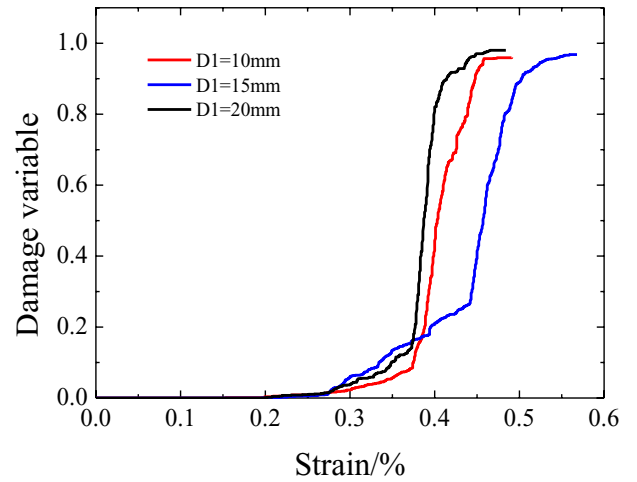


Figure 25. Damage variable-strain curves of specimens with different borehole depths.

$$K_d = K_w A_d = \frac{K_0}{A} A_d. \quad (5)$$

Hence,

$$D = \frac{K_d}{K_0}. \quad (6)$$

It is difficult to achieve absolute complete failure mode in the process of rock compression. Refer to [26, 27], the damage variable is corrected as

$$D = D_u \frac{K_d}{K_0} \quad (7)$$

where D_u is the critical damage value.

The damage threshold is normalized by the linear function transformation method:

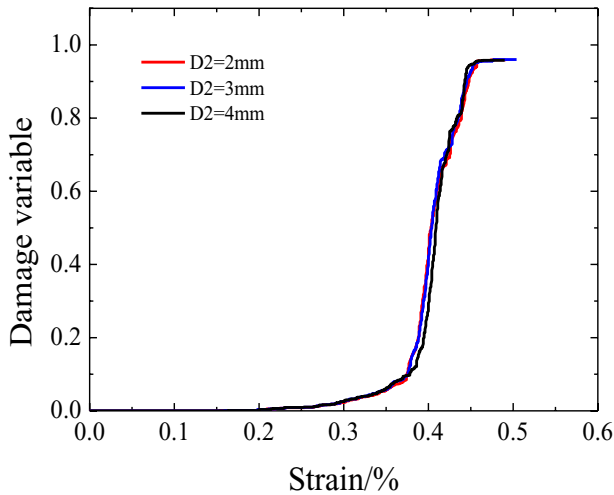


Figure 26. Damage variable-strain curves of specimens with different borehole diameters.

$$D_u = 1 - \frac{\sigma_c}{\sigma_p} \quad (8)$$

where σ_p is the peak intensity and σ_c is the residual intensity.

Based on AE impact characteristics and strain equivalence principle [28], the uniaxial compression damage constitutive model can be described as

$$\sigma = E\varepsilon(1 - D) = E\varepsilon \left(1 - D_u \frac{K_d}{K_0} \right). \quad (9)$$

Figure 22 shows the stress–strain fitting curve based on equation (9), which shows good agreement with the numerical calculation results.

4.2. Regular analysis of damage evolution

Figure 23 shows the damage evolution curve of the numerical granite. It can be seen that the damage evolution process can be divided into three stages. The first one is the damage stable development stage. In this stage, the damage variable gradually increases, and the initial crack of the rock gradually expands, and new crack is growing. The second stage is the damage accelerate development stage. The damage variable increases rapidly to the critical value. The micro cracks in the rock rapidly develop into joint fissures, and macroscopic damage appears. The third stage is the damage peak stationary stage, where the damage variable reaches the maximum and the rock gradually loses its bearing capacity.

4.2.1. Influence of the drilling hole position. Figure 24 shows the damage evolution curve of the numerical granite in different drilling hole position conditions. It can be seen that the influence of the drilling hole position on the damage evolution rule is mainly in the accelerated development and damage peak stationary stages. As the drilling hole position changes, the initial strain of the damage acceleration value is 0.28%. However, the slope of the initial acceleration damage increases gradually. As the drilling hole position changes from

top to bottom, the strain of the damage acceleration decreases gradually and the value is not large.

4.2.2. Influence of the drilling hole depth. Figure 25 depicts the damage evolution curve of the numerical granite in different drilling hole depths conditions. The drilling depth influences the damage evolution mainly in the accelerated development and damage peak stationary stages. As the drilling depth increases, the initial strain of the damage acceleration phase is 0.26% and is maintained. However, the slope of the initial damage increases initially and decreases afterwards, while the slope of the acceleration damage decreases initially and increases afterwards. When the drilling hole depth is 15 mm, the continuous strain range of the initial damage slope is the biggest and the range values are 1.5 times the 10 and 20 mm depths. The strain values in the damage peak stationary stage increases initially and decreases afterwards with the increases of the drilling hole depth. Hence, the evolution path of rock damage evolution curve is different at different drilling hole depths.

4.2.3. Influence of the drilling hole diameter. Figure 26 illustrates the damage evolution curve of the numerical granite in different drilling hole diameters conditions. It observes that the drilling hole diameter has little effect on the damage evolution law.

Overall, the characteristics of rock damage evolution with different drilling hole positions, depths and diameters are different. The importance order is position, depth and diameter factors.

5. Conclusion

This paper takes granite geology as the engineering background. The influence of different drilling hole positions, depths and diameters on rock mechanics and AE characteristics is explored based on the PFC2D numerical model. Important parameters such as the drilling hole position, depth and diameter are systematically analyzed in the pressure relief process. The following conclusions can be drawn.

- (1) The drilling hole position has little influence on the elastic stage of the numerical granite stress–strain curve but exhibits some influence on the plastic deformation and the damage residual stages. The peak strength and peak strain of the numerical granite were decreasing with the top and bottom of the drilling hole positions, but the elastic modulus was basically unchanged. The drilling hole depth has certain influence on the elastic stage, plastic deformation stage and damage residual stage of the numerical granite stress–strain curve. The peak strength and elastic modulus of the numerical granite decreased continuously. The peak strain shows a tendency to decrease first and then increase. Drilling hole diameter has less influence on the whole three stress–strain stages.
- (2) The strain value of the initial AE, the impact strength of the peak moment AE, the strain range of the strong AE impact, the fluctuations of AE, the induction time of AE



and the maximum impact time were all affected by the drilling hole position and the drilling hole depth. As the drill position moved from top to bottom, the following phenomenon occurred: the strain value of the initial AE decreased continuously, the impact intensity of AE at peak time was decreasing, the strain range that produces stronger AE impact increased continuously, the time for initiating the initial AE was reduced and the time that produces the loudest launch had a tendency to increase first and then decrease. As the drilling hole depth increased, the following phenomenon occurred: the strain value induced by initial AE increased, the impact intensity of AE at peak time increased, fluctuation was complicated first and then became simple, the strain range that produces the stronger AE impact had the tendency to increase first and then decrease and there was a tendency for the duration of the intense AE to be shorter and shorter. The drilling hole diameter had less influence on AE characteristics.

- (3) It may be observed that the influence of the drilling hole depth and the drilling hole position on the damage evolution rule of numerical granite is mainly in the accelerated development and damage peak stable stages. As the drilling hole position changes from top to bottom, the initial strain of the damage acceleration value is 0.28% and it also remains basically unchanged. However, the slope of the initial acceleration damage increases gradually. Subsequently, the accelerated damage slope has the tendency of gradually decreasing with the drilling hole from top to bottom. There is an increasing trend of strain value at the moment of the peak of damage and the peak plateau duration gets shorter and shorter. As the drilling hole depth increases, the initial strain of the damage acceleration phase is 0.26% and it is also basically unchanged. The slope of the initial acceleration damage increases initially and decreases afterwards; the slope of the acceleration damage decreases initially and increases afterwards. The strain values of the damage peak stable stage increase initially and decrease afterwards when the drilling hole depth increases. The drilling hole diameter has little effect on damage evolution.

Acknowledgments

This research is supported by the National Science Foundation of China (Nos. U1710258 and U1806229), Fundamental Research project of Central Universities (2019041008), Shanxi Province Technology Innovation Program for the Excellent Talents (No. 201605D211003), State Key Laboratory Cultivation Base for Mine Disaster Prevention and Control (MDPC201605211003) and Australia ARC DECRA (No. DE190100931).

ORCID iDs

Zhixiong Li  <https://orcid.org/0000-0002-7265-0008>
Weihua Li  <https://orcid.org/0000-0002-6190-8421>

References

- [1] Mohamed K M *et al* 2016 Analysis of the current rib support practices and techniques in U.S. coal mines *Int. J. Min. Sci. Technol.* **26** 77–87
- [2] Wang X, Wen Z J and Jiang Y J 2016 Time–space effect of stress field and damage evolution law of compressed coal-rock *Geotech. Geol. Eng.* **34** 1933–40
- [3] Obert L and Duvall W I 1967 *Rock Mechanics and the Design of Structures in Rock* (New York: Wiley) p 260
- [4] Wang C *et al* 2015 Predicting rockburst tendency based on fuzzy matter–element model *Int. J. Rock Mech. Min. Sci.* **75** 224–32
- [5] Xi W *et al* 2018 A feature extraction and visualization method for fault detection of marine diesel engines *Measurement* **116** 429–37
- [6] Jiang Y *et al* 2016 On the bi-dimensional variational decomposition applied to nonstationary vibration signals for rolling bearing crack detection in coal cutters *Meas. Sci. Technol.* **27** 065103
- [7] Li Z *et al* 2018 Multi-dimensional variational mode decomposition for bearing-crack detection in wind turbines with large driving-speed variations *Renew. Energy* **116** 55–73
- [8] Tang B 2000 Rock-burst control using destress blasting *PhD Thesis* McGill University, Montreal
- [9] Konicek P, Saharan M R and Mitri H 2011 Destress blasting in coal mining—state-of-the-art review *Proc. Eng.* **26** 179–94
- [10] Huang W P *et al* 2018 An innovative support technology employing a concrete-filled steel tubular structure for a 1000 m-deep roadway in a high *in situ* stress field *Tunn. Undergr. Space Technol.* **73** 26–36
- [11] Liu J H, Jiang F X and Wang N G 2013 *Control of Disasters Resulting from Roof Movement of Barge Fully Mechanized Caving Face with Deep Alluvium* (Beijing: Science Press)
- [12] Wang M, Wang X Y and Xiao T Q 2017 Borehole destressing mechanism and determination method of its key parameters in deep roadway *J. China Coal Soc.* **42** 1138–45
- [13] Li J K *et al* 2009 Numeric simulation of borehole pressure relief preventing roadway rockburst of a mine *J. Xi'an Univ. Sci. Technol.* **29** 424–32
- [14] Wen Y L, Zhang G J and Zhang Z Q 2013 Numerical experiments of drilling pressure relief preventing roadway rock burst *Appl. Mech. Mater.* **353** 1583–7
- [15] Jia C Y *et al* 2017 Laboratory and numerical experiments on pressure relief mechanism of large-diameter boreholes *Chin. J. Geotechn. Eng.* **39** 1115–22
- [16] Rudajev V, Vilhelm J and Lokajiček T 2003 Laboratory studies of acoustic emission prior to uniaxial compressive rock failure *Int. J. Rock Mech. Min. Sci.* **37** 699–704
- [17] Ishida T, Kanagawa T and Kanaori Y 2010 Source distribution of acoustic emissions during an *in situ* direct shear test: implications for an analog model of seismogenic faulting in an inhomogeneous rock mass *Eng. Geol.* **110** 66–76
- [18] Cundall P A and Strack O D 1979 A discrete numerical model for granula assemblies *Geotechnique* **29** 47–65
- [19] Itasca Consulting Group 2008 *PFC2D (Particle Flow Code in 2 Dimensions) Fish in PFC2D* (Minneapolis: Itasca Consulting Group)
- [20] Khazaei C, Hazzard J and Chalaturnyk R 2016 A discrete element model to link the microseismic energies recorded in caprock to geomechanics *Acta Geotech.* **11** 1351–67
- [21] Zhang X P *et al* 2014 Simulation research on granite compression test based on particle discrete element model *Rock Soil Mech.* **35** 99–105

- [22] Hazzard J F, Young R P and Maxwell S C 2000 Micro-mechanical modeling of cracking and failure in brittle rocks *J. Geophys. Res.* **105** 1978–2012
- [23] Wang X *et al* 2018 Experimental study on mechanical and acoustic emission characteristics of rock-like material under non-uniformly distributed loads *Rock Mech. Rock Eng.* **51** 729–45
- [24] Liu X W, Lin J Z and Yuan Z Y 1997 Research on evaluation of material fatigue damage by acoustic emission technology *China Railway Sci.* **18** 74–91
- [25] Kachanov L M 1958 Time rupture process under creep conditions *Izv. Akad. Nauk SSSR, Otd. Tekhnicheskich Nauk* **8** 26–31
- [26] Liu B X *et al* 2009 Study on damage evolution and acoustic emission character of coal-rock under uniaxial compression *Chin. J. Rock Mech. Eng.* **28** 3234–8
- [27] Zong Y *et al* 2016 Mechanical and damage evolution properties of sandstone under triaxial compression *Int. J. Min. Sci. Technol.* **26** 601–7
- [28] Lemaitre J, Sermage J P and Desmorat R 1999 A two scale damage concept applied to fatigue *Int. J. Fract.* **97** 67–81